Journal of Fluids and Structures 18 (2003) 23–42

JOURNAL OF FLUIDS AND STRUCTURES

www.elsevier.nl/locate/jnlabr/yjfls

Random binary (coalescence) flutter of a two-dimensional linear airfoil

D. Poirel[a,*], S.J. Price[b]

[a] *Department of Mechanical Engineering, Royal Military College of Canada, PO Box 17000, Station Forces Kingston, Ontario, K7K 7B4 Canada*

[b] *Department of Mechanical Engineering, McGill University, 817 Sherbrooke Street West, Montréal, Québec, H3A 2K6 Canada*

Received 22 November 2001; accepted 12 June 2003

Abstract

The binary flutter mechanism of a two-dimensional linear airfoil (typical section) in turbulent flow is investigated numerically. The airfoil is modelled as a flexibly mounted rigid flat plate, with degrees of freedom in pitch and heave. The unsteady aerodynamics is represented using both Wagner's function, accounting for arbitrary motion and longitudinal turbulence, and küssner's function, accounting for vertical turbulence. The flutter stability/instability boundary is examined according to the concept of sample stability, as given by the largest Lyapunov exponent. Results show that, for all airfoil and turbulence parameters considered, the longitudinal component of turbulence lowers the flutter speed. This decrease in flutter speed is determined essentially by the small and very small frequencies of the turbulence excitation, specifically due to principal and secondary combination difference type parametric resonances. Furthermore, there is strong evidence that the random excitation, specifically the longitudinal component, modifies the modal characteristics of the system, and in turn the coalescence of the two aeroelastic modal frequencies. In this sense, the nature of the shift of the flutter point is typical of the deterministic classical binary flutter problem.
Crown Copyright © 2003 Published by Elsevier Ltd. All rights reserved.

1. Introduction

In previous papers (Poirel and Price, 1997, 2001) we explored different aspects of the dynamics of a structurally nonlinear two-dimensional airfoil (the typical section) in turbulent flow. In particular, some characteristics of the supercritical Hopf bifurcation were investigated and interpreted from the point of view of random bifurcation theory. Briefly, random bifurcation theory defines two basic types of bifurcation: the D- (for Dynamical) and P- (for Phenomenological) bifurcations. The D-bifurcation corresponds to a loss of stability as expressed by a change of sign of the largest Lyapunov exponent; hence, it is associated with a critical slow down of the dynamics in the same manner as for the deterministic dynamics. Note, that the Lyapunov exponents are a generalization of the real part of the eigenvalues, defined for a fixed point, to any arbitrary solution. On the other hand, the P-bifurcation defines a qualitative change in the dynamical behaviour as represented by the probability density function of the response. For the special case of the (trivial) deterministic problem, the D- and P-bifurcation points coincide at one airspeed; in other words, the largest Lyapunov exponent vanishes at the same airspeed as the limit cycle oscillation appears.

It was found that under pure longitudinal excitation (which acts as a random parametric excitation) the bifurcation becomes a two-step bifurcation, characterized by: first, a D-bifurcation, followed by a P-bifurcation. The D-bifurcation was associated with the flutter speed, and the P-bifurcation with the onset of the limit cycle oscillation. When vertical

*Corresponding author. Tel.: +1-613-541-6000; fax: +1-613-542-8612.
E-mail address: poirel-d@rmc.ca (D. Poirel).

0889-9746/$ - see front matter Crown Copyright © 2003 Published by Elsevier Ltd. All rights reserved.
doi:10.1016/S0889-9746(03)00074-4

Nomenclature

a_h	nondimensional distance between elastic axis and midchord
b	semichord
h, θ	airfoil motion in heave and pitch directions
I_{EA}	airfoil moment of inertia about elastic axis
K_h, K_θ	heave and pitch stiffness coefficients
k	reduced frequency, $\omega b/U_m$.
k_f	deterministic flutter reduced frequency
L_{nd}	nondimensional scale of turbulence, L/b
$L(t), M_{EA}$	lift force and aerodynamic moment about the elastic axis
m	airfoil mass per unit length
r_θ	nondimensional radius of gyration, I_{EA}/mb^2
U	total freestream velocity, $U_m + u_T$
U_{nd}	nondimensional speed, $U/b\omega_\theta$
U_m	mean freestream velocity
$U_{m,nd}$	nondimensional mean freestream velocity
$U_{f,nd}$	nondimensional deterministic flutter speed
u_T, w_T	longitudinal and vertical turbulence velocities
$u_{T,nd}, w_{T,nd}$	nondimensional turbulence velocities
$\bar{u}, \bar{w}$	normalized turbulence velocities, $u_{T,nd}/U_{m,nd}$, $w_{T,nd}/U_{m,nd}$
t, s	time
$w_{3/4}$	downwash at three-quarter chord
x_θ	nondimensional distance between elastic axis and centre of mass
z_1, z'_1	nondimensional aerodynamic lag states due to Wagner's function
z_2, z'_2	nondimensional aerodynamic lag states due to Küssner's function
α	angle of attack
μ	nondimensional airfoil mass, $m/\rho\pi b^2$
ξ	nondimensional heave motion, h/b
$\Lambda_{\max}$	largest Lyapunov exponent
$\lambda_{\max}$	nondimensional largest Lyapunov exponent, $\Lambda_{\max} b/U_m$
ρ	density of air
σ_T^2	turbulence velocity variance
$\sigma_{T,nd}^2$	nondimensional turbulence velocity variance, $\sigma_T^2/(b\omega_\theta)^2$
τ	nondimensional time, $U_m t/b$
ϕ_{LT}, ϕ_{VT}	longitudinal and vertical turbulence power spectral densities
$\Phi(t)$	Wagner's function
$\Psi(t)$	Küssner's function
ω	radial frequency
ω_h, ω_θ	radial frequencies in heave and pitch
$\bar{\omega}$	frequency ratio, ω_h/ω_θ
$(\cdot)$	derivative with respect to dimensional time
$()'$	derivative with respect to nondimensional time, $\mathrm{d}/\mathrm{d}\tau$

turbulence is added (it takes the form of a random external forcing), the D-bifurcation disappears and only the P-bifurcation remains.

We also reported preliminary results concerning the stability and response behaviour of the turbulent excited airfoil in its linear form. We found that for the few cases studied the stability of the linear airfoil, strictly speaking its fixed point, is lost via a D-bifurcation, which, due to longitudinal turbulence, occurs at a lower airspeed compared with the deterministic flutter speed. It was also shown (Poirel, 2001) that, contrary to the nonlinear airfoil, vertical turbulence does not affect the D-bifurcation of the linear airfoil; in fact, for the general linear problem, the external forcing does not contribute to or affect the system stability. Furthermore, it was shown that longitudinal turbulence caused the airfoil to respond with more intensity to vertical excitation. This occurred not only in the close vicinity of the flutter

point, but at all airspeeds. We therefore concluded that longitudinal turbulence decreases the stability of the airfoil on two accounts. Not only does it reduce the flutter speed, but it also diminishes the damping for airspeeds below flutter. This was corroborated by the behaviour of the largest Lyapunov exponent, which is closer (less negative) to the neutral axis at all (pre-flutter) airspeeds.

In this paper we restrict the analysis to the linear problem, and examine more closely the binary flutter characteristics of the turbulent excited airfoil. We confirm and generalize our previous preliminary results by presenting a systematic analysis for different combinations of turbulence and airfoil parameters. We also shed some light on other aspects of the random coalescence flutter and analyse the problem in terms of parametric resonance. Furthermore, a brief overview of random flutter is presented with the objective of putting in perspective specific issues related to this problem. In short, a primary objective is to present a more complete picture, and gain a more fundamental understanding, of the effect of longitudinal turbulence on the loss of stability of the fixed point due to coalescence flutter.

Contrary to the deterministic problem, where the observation of a signal often leaves (relatively) very little room for interpretation, the determination of stochastic stability is, in general, not a trivial affair. It is therefore relevant to briefly introduce some fundamental aspects of stochastic stability before discussing random flutter. Due to the innate random nature of a stochastic system (or random since, according to Arnold (1998), the qualifying term "stochastic" applies to problems where the excitation is white, whereas "random" refers to coloured noise excited problems), the most viable approaches are obviously probabilistic and statistical. Hence, in an effort to create a manageable approach to the problem, the different concepts of stochastic stability have been defined along these lines; the two main, fundamental, concepts are sample stability and moment stability.

Sample stability (also termed almost sure stability, almost certain stability, or stability with probability one) describes the stability in terms of probability, and ensures the stability of all sample functions except for those whose probability of occurrence is negligible. For instance, Mitchell and Kozin (1974) express almost sure asymptotic sample stability of the trivial solution, $x = 0$, as

$$P[\lim_{t\to\infty} ||x(t)|| \to 0] = 1. \tag{1}$$

Consider the linear stochastic system $\dot{x} = A(\xi(t))x$ in $\mathbb{R}^d$, where $\xi(t)$ is a stationary ergodic random process given by the solution of

$$\mathrm{d}\xi = a\xi\,\mathrm{d}t + b\,\mathrm{d}W \tag{2}$$

and W is the Weiner process on the probability space $\{\Omega, \tau, P\}$. The Lyapunov exponent of a solution $x(t, x_0)$ is defined by

$$\lambda(x_0) = \lim_{t\to\infty} \frac{1}{t}\log||x(t, x_0)||, \quad x(0) = x_0. \tag{3}$$

It represents the average exponential growth rate of the solution $x(t, x_0)$. In general, the Lyapunov exponent is a random variable which, according to Oseledec's multiplicative ergodic theorem, and under certain assumptions such as ergodicity, takes only a finite number of nonrandom values $\lambda_p < \lambda_{p-1} < \ldots < \lambda_1 = \lambda_{\max}$, $p \leqslant d$. Furthermore, under assumptions related to differential operators it can be shown that

$$\lambda_{\max} = \lambda(x_0) = \lim_{t\to\infty} \frac{1}{t}\log||x(t, x_0)||, \quad \text{with probability 1}, \tag{4}$$

where $\lambda_{\max}$ is nonrandom and independent of x_0. The reader is referred to Arnold et al. (1986) for details of the theorems and conditions. Sample stability is therefore controlled by the value of the largest Lyapunov exponent, $\lambda_{\max}$, such that a change in sign of $\lambda_{\max}$ (from negative to positive) corresponds to a loss of stability, almost surely, of the fixed point (Baxendale, 1991; Arnold et al., 1986). As introduced earlier, a vanishing $\lambda_{\max}$ is also indicative of a D-bifurcation (Arnold, 1995).

The other main notion used to describe stochastic stability is in terms of a statistical functional of samples. Here, we introduce the older concept of moment stability. According to Mitchell and Kozin (1974), the trivial solution is considered asymptotically stable in the nth-moment if the following condition is met:

$$\lim_{t\to\infty} \mathrm{E}[||x(t)||^n] \to 0, \tag{5}$$

where $||x(t)||$ is the Euclidian norm of a point on the d-dimensional trajectory, and E[ ] is the expectation or the ensemble average. Although n can take different values, it is common to concentrate on the traditional second moment ($n = 2$), thus mean-square stability, which provides a better physical insight than that obtained with other values of n.

In general, moment stability does not imply sample stability and vice versa. However, it has been shown that, for linear stochastic differential equations, conditions ensuring mean-square stability are more stringent than those

required for sample stability. In other words, mean-square stability implies sample stability. Conversely, a stochastic system which is not almost surely stable (sample stability) is also unstable in the mean-square sense; for example, see Mitchell and Kozin (1974) or Lin (1996). Note that in this paper the random flutter point is identified according to a change in sign of $\lambda_{\max}$. We are therefore concerned with sample stability, and by extension with the D-bifurcation.

2. Overview of random flutter in aeroelasticity

In order to have a better understanding of the mechanisms that dictate the effect of longitudinal turbulence on the instability it is relevant to first underline the specific nature of coalescence flutter in contrast to other flutter instabilities. This discussion is also motivated by the observation that in the relatively recent literature concerning random flutter, either in aeroelasticity or in fluidelasticity (fluid–structure interaction), often the type of flutter being examined is neither stated clearly nor can it be deduced easily. Before going further, it is essential to recognize that the type of problem being discussed in this paper is time-varying (or parametrically excited), i.e. the parameters are fluctuating (randomly) in time, as opposed to a time-invariant system with uncertain (nondeterministic) parameters. Accordingly, the term "random" flutter does not refer to the flutter speed being a random variable, but to the random nature of the excitation. In fact, the flutter speed is considered to be a deterministic variable for the problem discussed in this paper.

From a mathematical point of view, flutter instabilities are dynamical instabilities which can be described by a pair of complex conjugate eigenvalues whose real part vanishes at the flutter speed. However, the physical origin of each type of flutter instability can be significantly different. From a fundamental point of view it is generally considered that there are two broad classes of flutter. One is sometimes referred to as fluid-stiffness-controlled instability, which requires at least two-degrees-of-freedom or modes of vibration to exist. This is the case treated here. It is characterized by a near (but not exact) coalescence of two aeroelastic modal frequencies. The ratio of the two uncoupled natural frequencies, $\bar{\omega}=\omega_h/\omega_\theta$, has a strong influence on the airspeed at which this instability occurs. It is therefore highly sensitive to the system stiffness properties, but much less sensitive to the system damping. Unsteady aerodynamics is not required to qualitatively represent this instability; it can be predicted using quasi-steady aerodynamics. This type of flutter is also termed coalescence, binary, two-degree-of-freedom, two-mode or classical flutter. It is not restricted to airfoils, and can be found on other structures; such as: arrays of flexible tube bundles, panels (hence panel flutter) or bridges.

The other broad class of flutter is a fluid-damping-controlled instability. One sub-class is called single-degree-of-freedom flutter. In its simplest form it involves one-degree-of-freedom only, which for an airfoil must be in torsion. Furthermore, in order to predict negative aerodynamic damping the analysis must properly model the unsteady aerodynamics. This single-degree-of-freedom flutter is, however, a rare occurrence. More common is stall-flutter, which can occur either in bending or in torsion, although the physical mechanism is slightly different in each case. As the name suggests, for stall-flutter separated flow must exist in both cases. The torsional motion instability requires dynamic stall to have occurred, hence accurate modelling of both unsteady aerodynamics and separated flow is required. The bending motion can become unstable simply due to a negative lift curve slope associated with static stall. One additional fundamental difference between stall and coalescence flutter is that, due to its inherent nonlinear nature, stall-flutter does not only refer to the loss of stability of an equilibrium point, but also to the post-instability dynamics in the form of an LCO. In contrast, coalescence flutter describes purely the loss of stability.

An important class of aeroelastic problems where random (and stochastic) flutter has been studied previously concerns bridges in turbulent wind (Bucher and Lin, 1988a, b, 1989; Lin and Li, 1993; Li and Lin, 1995; Lin, 1996). The vast majority of their work concentrated on the analytical treatment of single-degree-of-freedom type instabilities, mainly negative-damping flutter. They found, on the basis of a single-degree-of-freedom model, that longitudinal turbulence is generally destabilizing, whereas it could have a stabilizing effect if coupling with additional modes of vibration was accounted for. Li and Lin (1995) and Lin (1996) also highlighted the significance of the excitation at frequencies corresponding to $2\omega_1$, twice the flutter frequency (i.e. principal parametric resonance), and $|\omega_1-\omega_2|$(i.e. parametric combination, difference type, resonance) for the two-degree-of-freedom case.

We have found only one clear instance where the coalescence (binary or two-mode) flutter of a bridge is treated (Bucher and Lin, 1988b), albeit very superficially. Their analysis showed a destabilizing effect, in the mean-square sense, of longitudinal turbulence on this type of flutter. Furthermore, the degree of destabilization appears, essentially, to be proportional to the excitation spectral density.

Another important example of random flutter in aeroelasticity is that of helicopter rotor blades in turbulent flow. This has been studied by Lin et al. (1979), Fujimori et al. (1979), Prussing and Lin (1982, 1983). Of particular interest is the torsion-flap problem, which is similar to the binary flutter treated in this paper (Done, 1996), except for the added

periodic parametric excitation originating from forward flight (Fujimori et al., 1979). Considering the excitation as white noise, modelling the aerodynamics as quasi-steady, and neglecting the quadratic noise component, u_T^2, it was found by Fujimori et al. (1979) that in-plane (longitudinal) turbulence had a destabilizing effect, in the mean-square sense, for this type of flutter.

Our discussion also adds to the work of Ibrahim et al. (1990, 1991) on stochastic panel (two-mode) flutter. Using a structural model with two or three modes, assuming quasi-steady supersonic aerodynamics, and considering a parametric white noise excitation originating from structural in-plane loads and acting on the stiffness terms only, they found that parametric random excitation was always destabilizing in the mean-square sense.

The more general fluid–structure interaction (fluidelasticity) scenario also lends itself to the study of the effect of upstream turbulence on flexible tubes in cross-flow, a topic which has and still receives a lot of attention, for example Romberg and Popp (1998). This is an extremely vast domain of research and no attempt will be made to provide even a modest overview of the problem.

3. Problem modelling

The typical section, also known as the two-dimensional airfoil, is used for this analysis. This is shown schematically in Fig. 1. The airfoil is modelled as a rigid flat plate, with degrees of freedom in pitch and heave. Structural flexibility is provided by torsional and translational springs. Structural damping is neglected. The model is linear and represented by the following two coupled differential equations (Fung, 1955), heave being defined positive down and pitch nose up:

$$I_{EA}\ddot{\theta} + mx_\theta b\ddot{h} + K_\theta\theta = M_{EA}(t), \tag{6a}$$

$$mx_\theta b\ddot{\theta} + m\ddot{h} + K_h h = -L(t). \tag{6b}$$

In addition to the parameters and variables shown in Fig. 1, I_{EA} represents the mass moment of inertia about the elastic axis, and m is the airfoil mass. K_θ and K_h are the torsional and translational linear spring coefficients, respectively. The uncoupled structural natural frequencies in heave and pitch, respectively, are $\omega_h = (K_h/m)^{1/2}$ and $\omega_\theta = (K_\theta/I_{EA})^{1/2}$. Coupling between the two degrees-of-freedom arises from the inertia terms when the elastic axis and centre of mass are not coincident ($x_\theta \neq 0$), and otherwise from the aerodynamics. On the right-hand side of the pitch and heave equations are the aerodynamic moment about the elastic axis and lift force, respectively. Also shown in Fig. 1 are the mean airspeed and the two turbulence velocities, longitudinal and vertical.

Details of the aerodynamic modelling and representations of the turbulence are given in the following sections.

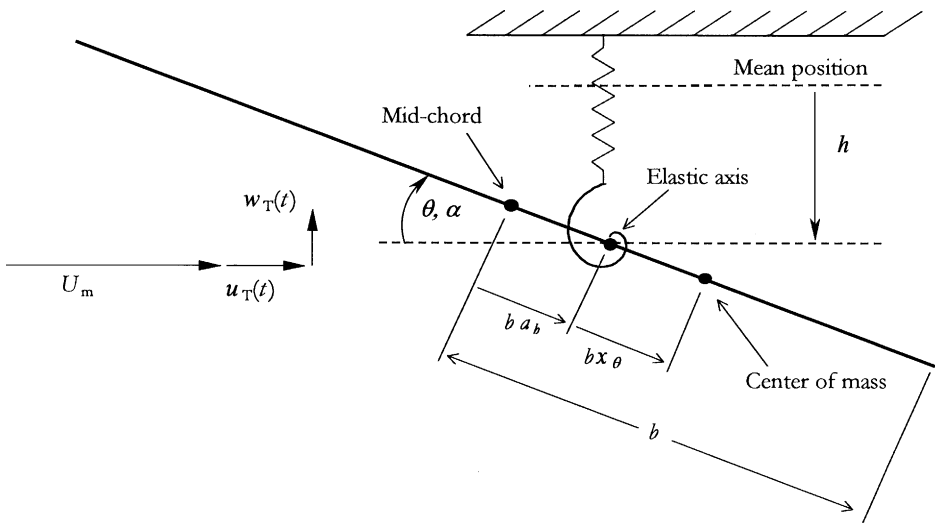

Fig. 1. Schematic of the two-dimensional airfoil model.

3.1. Turbulence model

The random excitation is modelled using the Dryden continuous turbulence model (Hoblit, 1988; Houbolt et al., 1964). Some important simplifying assumptions employed in this model are: a Gaussian distribution of fluctuating velocities; chordwise (only used for the longitudinal component) and vertical uniformity; isotropy and statistical stationarity. Furthermore, it is assumed that temporal gradients of the turbulent velocity fluctuations are negligibly small compared to the gradients along the flight path (in x, $\bar{x}$) of the airfoil. This is known as Taylor's (and von Kármán's) hypothesis, or the frozen turbulence assumption. It is formulated as $u_T = u_T(\bar{x}, \bar{y}, \bar{z}, t) = u_T(\bar{x}, \bar{y}, \bar{z}) = u_T(x - U_m t, y, z)$, where $(\bar{x}, \bar{y}, \bar{z})$ and (x, y, z) form atmospheric and body fixed coordinate systems, respectively. It is then possible to convert spatial variables into time, such that the turbulent velocities are considered statistically stationary with respect to time in the body fixed coordinate system. Since this work is restricted to the two-dimensional airfoil, only the longitudinal and vertical components of turbulence are relevant, respectively, $u_T = u_T(t)$ and $w_T = w_T(t)$. As a result of the longitudinal excitation, the airspeed is time-varying.

The basic representation of the Dryden model is given in the frequency domain, as shown in Eq. (7a) and (b) for the longitudinal and vertical turbulent velocity power spectral densities (PSDs), respectively:

$$\phi_{uu}(\omega) \equiv \phi_{LT}(\omega) = \sigma_T^2 \left(\frac{2L}{\pi U_m}\right) \frac{1}{1 + [L\omega/U_m]^2}, \tag{7a}$$

$$\phi_{ww}(\omega) \equiv \phi_{VT}(\omega) = \sigma_T^2 \left(\frac{L}{\pi U_m}\right) \frac{1 + 3[L\omega/U_m]^2}{[1 + [L\omega/U_m]^2]^2}. \tag{7b}$$

These spectra are presented in nondimensional form in Fig. 2 for a scale of turbulence and variance, $L_{nd} = 50.0$ and $\sigma^2_{T,nd} = 10$, respectively. The scale of turbulence, L, divided by the mean free-stream velocity, U_m, is equal to the correlation time of the longitudinal random excitation (in nondimensional form they are equal, $L_{nd} = \tau_{\mathrm{cor}}$). The scale of turbulence can be interpreted physically as the "average" distance travelled by the airfoil during which the turbulence velocities can be considered as uniform. Hence, the larger the scale of turbulence, the farther, in average, the airfoil travels before experiencing a change in turbulence velocities.

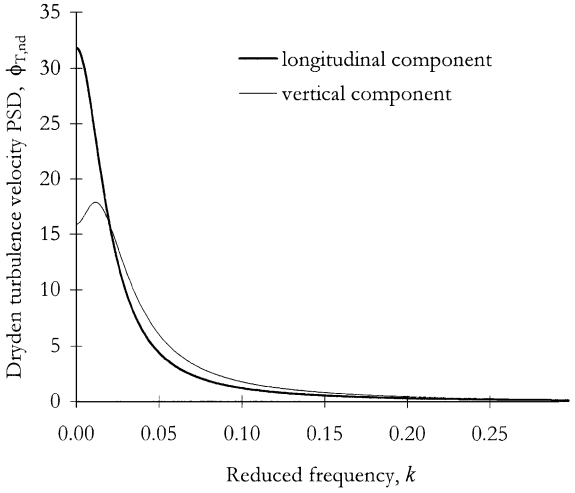

Fig. 2. Closed-form solution of the nondimensional PSD of Dryden turbulence; $L_{nd} = 50.0$ and $\sigma^2_{T,nd} = 1.0$.

In order to practically implement the Dryden excitation as an input to the aeroelastic system, specifically into the lift force and aerodynamic moment, the excitation must be transformed into the time domain. The procedure consists of developing a transfer function in the Laplace domain that relates unit (i.e. $\phi_{WN} = 1$) Gaussian white noise as input and the turbulence velocity as output. The square of the modulus of the transfer function, expressed in the frequency domain, must match the turbulence PSD given in Eq. (7). In essence, Eq. (7) is a filter between white noise and the proper excitation. Taking the inverse Laplace transform of the transfer functions gives the following time domain

representation:

$$\mathrm{d}u_T + \frac{U_m}{L}u_T\mathrm{d}t = \sigma_T\left(\frac{2U_m}{\pi L}\right)^{1/2}\mathrm{d}W_1, \tag{8a}$$

$$\mathrm{d}w_T + \frac{2U_m}{L}w_T\,\mathrm{d}t + \frac{U_m^2}{L^2}\left(\int_0^t w_T\,\mathrm{d}s\right)\mathrm{d}t = \sigma_T\left(\frac{U_m^3}{\pi L^3}\right)^{1/2}\left(\int_0^t \mathrm{d}W_2\right)\mathrm{d}t + \sigma_T\left(\frac{3U_m}{\pi L}\right)^{1/2}\mathrm{d}W_2. \tag{8b}$$

As shown in Eq. (8), the longitudinal and vertical turbulence velocities act as dependent variables. On the r.h.s. are two statistically independent Weiner processes, W_1 and W_2 (the Weiner process is related to (unit) Gaussian white noise by $\mathrm{d}W = G_{WN}\,\mathrm{d}t$). Independence between the two processes is justified physically by the hypothesis of isotropy of the turbulent field. Note that Eq. (8) can be interpreted either in the Itô or Stratonovich sense since the noise is additive.

3.2. Aerodynamic model

Restricting the flow to being attached and incompressible, but accounting for unsteady (lag) effects, the aerodynamics is modelled as

$$\begin{aligned} L(t) = {} & \pi\rho b^2[\ddot{h} + U\dot{\alpha} - ba_h\ddot{\alpha}] + 2\pi\rho bU\left[w_{3/4}\Phi(0) - \int_0^t w_{3/4}(s)\frac{\mathrm{d}\Phi(t-s)}{\mathrm{d}s}\mathrm{d}s\right] \\ & + 2\pi\rho bU_m\left[w_T\Psi(0) - \int_0^t w_T(s)\frac{\mathrm{d}\Psi(t-s)}{\mathrm{d}s}\mathrm{d}s\right], \end{aligned} \tag{9a}$$

$$\begin{aligned} M_{EA}(t) = {} & \pi\rho b^2[ba_h\ddot{h} - b[0.5 - a_h]U\dot{\alpha} - b^2[a_h^2 + 1/8]\ddot{\alpha}] + 2\pi\rho b^2[a_h + 0.5]U\left[w_{3/4}\Phi(0) - \int_0^t w_{3/4}(s)\frac{\mathrm{d}\Phi(t-s)}{\mathrm{d}s}\mathrm{d}s\right] \\ & + 2\pi\rho b^2[a_h + 0.5]U_m\left[w_T\Psi(0) - \int_0^t w_T(s)\frac{\mathrm{d}\Psi(t-s)}{\mathrm{d}s}\mathrm{d}s\right], \end{aligned} \tag{9b}$$

where

$$w_{3/4}(t) = \dot{h} + U\alpha + b[0.5 - a_h]\dot{\alpha}, \tag{10}$$

$$U = U_m + u_T(t), \tag{11}$$

$$\Phi(t) = 1 - 0.165\mathrm{e}^{-0.0455U_m t/b} - 0.335\mathrm{e}^{-0.3U_m t/b}, \tag{12}$$

$$\Psi(t) = 1 - 0.5792\mathrm{e}^{-0.1393U_m t/b} - 0.4208\mathrm{e}^{-1.802U_m t/b}. \tag{13}$$

Both the lift force and aerodynamic moment are composed of three types of terms. Terms proportional to airfoil acceleration are added mass terms, which physically represent the reaction force of the air displaced by the accelerated motion of the airfoil. The second set of terms, those that are proportional to U, comprise the circulatory airloads, which model the effects of the bound vorticity and the shed wake. They account for arbitrary motion of the airfoil, as defined by the downwash at the three-quarter chord point, $w_{3/4}$. These terms are influenced by the turbulent excitation via the airspeed $U = U_m + u_T(t)$, which is composed of a constant mean part, U_m, and a time-varying component, $u_T(t)$, due to the longitudinal turbulence excitation. The unsteady effects are modelled by a two-state representation of Wagner's function, $\Phi(t)$, given by Eq. (12) (Fung, 1955). The final type of expression introduced in Eq. (9) is solely due to the vertical component of turbulence, $w_T(t)$. In this case, the unsteady effects are given by a two-state representation of Küssner's gust-penetrating function, $\psi(t)$, shown in Eq. (13). Additional details are provided by Poirel (2001).

The added mass and circulatory airload terms are similar to those given by Fung (1955), except that they have been modified, based on the work of van der Wall and Leishman (1994) and Dinyavari and Friedmann (1986), to include a random time-varying airspeed. One necessary simplifying assumption, relevant to both the bound vorticity and added mass, is chordwise uniformity of the longitudinal turbulence excitation. This can be justified physically in the limit of low frequency excitation, since the flow velocity gradients along the chord are small for small reduced frequencies.

Another notable simplifying assumption in the circulatory terms concerns the airspeed used in Wagner's function, which is assumed to be constant and set at the mean airspeed, U_m. This assumption effectively forces the distance travelled by the vortices in the wake to be equal to $U_m t$, thus airspeed fluctuations in the trailing wake are neglected. In support of this assumption, an heritage from Greenberg's original theory, Dinyavari and Friedmann (1986) argue that unsteady airloads are much more sensitive to the velocity of the wake vortices than their position. Furthermore, van der Wall and Leishman (1994) show that this is justified for a combination of low frequency and small amplitude airspeed variations. Furthermore, this assumption makes physical sense when it is realized that in these conditions the distance covered by the shed vortices is determined, in large part, by the mean airflow speed.

Due to the Gaussian nature of the excitation the model predicts that very high amplitude turbulent velocities may occur, resulting in a reversal of the flow over the airfoil. In this case the aerodynamic model breaks down. However, by virtue of the distribution shape, the very high amplitudes occur with a very low level of probability, such that, in practice and for the range of turbulence intensities studied in this paper, flow reversal occurs for a very short period of time and therefore can be effectively neglected. For example, a turbulent intensity $T_u = 25\%$ (i.e. $\sigma^2_{T,nd} = 1.0$ and $U_{m,nd} = 4.0$) has a probability of flow reversal $P(u_{T,nd} < -U_{m,nd}) = 0.00003$; assuming a frequency interpretation of probability, this means that flow reversal occurs for only 0.003% of the (flight) time and therefore will not affect significantly the overall predicted dynamics.

To show more specifically the effect of the longitudinal random excitation, the airspeed used in both the added mass and circulatory airloads due to arbitrary airfoil motion and the longitudinal turbulence is expanded for the lift force, shown in Eq. (9a), giving the following:

$$\begin{aligned}\pi\rho b^2[\ddot{h} + U\dot{\alpha} - ba_h\ddot{\alpha}] + 2\pi\rho bU\left[w_{3/4}\Phi(0) - \int_0^t w_{3/4}(s)\frac{\mathrm{d}\Phi(t-s)}{\mathrm{d}s}\,\mathrm{d}s\right] &= \pi\rho b^2[\ddot{h} + [U_m + u_T(t)]\dot{\alpha} - ba_h\ddot{\alpha}]\\ &+ 2\pi\rho b[[U_m + u_T(t)]\dot{h} + [U_m^2 + 2U_m u_T(t) + u_T^2(t)]\alpha + b[0.5 - a_h][U_m + u_T(t)]\dot{\alpha}]\Phi(0)\\ &- 2\pi\rho b[U_m + u_T(t)]\int_0^t \dot{h} + [U_m + u_T(s)]\alpha + b[0.5 - a_h]\dot{\alpha}\frac{\mathrm{d}\Phi(t-s)}{\mathrm{d}s}\,\mathrm{d}s. \end{aligned} \tag{14}$$

Note that the airspeed terms ($U = U_m + u_T$) are dependent on both the present time, t, and the historical time, s. In other words, the circulatory lift at time, t, is a function of the instantaneous value of the airspeed and its time history. Hence, the history of the longitudinal turbulence is represented by the $u_T(s)$ term. Examining Eq. (14) shows that the airfoil is excited by longitudinal turbulence in three different ways: these being the $u_T(t)$, $u_T^2(t)$ and $u_T(t)\,u_T(s)$ terms. The two nonlinear noise terms make the problem extremely difficult, if not impossible, to resolve analytically, but are easily handled numerically.

Eq. (14) is very similar to the one developed by Bucher and Lin (1988a, b) for the stability analysis of bridges in turbulent flow, with two notable exceptions. One difference is that the instantaneous airspeed, $U(t) = U_m + u_T(t)$, outside the integral in Eq. (14) is taken inside the integral in their analysis. This is done without justification. It can be attributed to the fact that they did not introduce the airspeed fluctuations at the source of their derivation, but instead at the end. The formulation of Bucher and Lin is thus theoretically questionable. We have, however, in the course of this work run a few test cases with their model and found no important numerical differences with ours, which indicates a certain robustness of the aerodynamic model. The second difference is that, on the basis of low turbulence intensity, Bucher and Lin neglected all quadratic noise terms, u_T^2, in order to obtain an analytical solution. We have also investigated numerically this aspect of their work, and found that the influence of u_T^2 is secondary even at a relatively high turbulence intensity, i.e. $T_u = 25\%$.

4. Numerical simulation

The aeroelastic equations of motion are formed by combining the structural equations of motion, Eq. (6), with the aerodynamic lift force and moment expressions, Eq. (9), which gives a set of two integro-differential equations. The numerical integration of this system can be facilitated by transforming the integral terms into differentials with the addition of two new second-order differential equations. Each additional second-order equation corresponds to two augmented states, given by z_1, z_1', z_2 and z_2', a consequence of the two-state representation chosen for Wagner's and Küssner's functions, respectively. Details of this process are given in Poirel (2001); see also Dinyavari and Friedmann (1986).

The transformation of the aeroelastic equations into pure differential form enables a physical interpretation of the different terms from the point of view of a traditional mechanical model with inertia, damping and stiffness forces and

external forcing. The nondimensional aeroelastic equations of motion are given below in differential form.

$$
\begin{bmatrix}
1+\dfrac{a_h^2+1/8}{\mu r_\theta^2} & \dfrac{x_\theta}{r_\theta^2}-\dfrac{a_h}{\mu r_\theta^2} & 0 & 0\\
x_\theta-\dfrac{a_h}{\mu} & 1+\dfrac{1}{\mu} & 0 & 0\\
0 & 0 & 1 & 0\\
0 & 0 & 0 & 1
\end{bmatrix}
\begin{Bmatrix} \theta'' \\ \xi'' \\ z_1'' \\ z_2'' \end{Bmatrix}
$$

$$
+\begin{bmatrix}
\dfrac{(1+\bar{u})(0.5-a_h)(1-(a_h+0.5))}{\mu r_\theta^2} & -\dfrac{(1+\bar{u})(a_h+0.5)}{\mu r_\theta^2} & -\dfrac{0.216015(1+\bar{u})(a_h+0.5)}{\mu r_\theta^2} & -\dfrac{0.838964(a_h+0.5)}{\mu r_\theta^2}\\
\dfrac{(1+\bar{u})}{\mu}+\dfrac{(1+\bar{u})(0.5-a_h)}{\mu} & \dfrac{(1+\bar{u})}{\mu} & \dfrac{0.216015(1+\bar{u})}{\mu} & \dfrac{0.838964}{\mu}\\
-(0.5-a_h) & -1 & 0.3455 & 0\\
0 & 0 & 0 & 1.9413
\end{bmatrix}
\begin{Bmatrix} \theta' \\ \xi' \\ z_1' \\ z_2' \end{Bmatrix}
$$

$$
+\begin{bmatrix}
\dfrac{1}{U_{m,nd}^2}-\dfrac{(1+\bar{u})^2(a_h+0.5)}{\mu r_\theta^2} & 0 & -\dfrac{0.01365(1+\bar{u})(a_h+0.5)}{\mu r_\theta^2} & -\dfrac{0.5020372(a_h+0.5)}{\mu r_\theta^2}\\
\dfrac{(1+\bar{u})^2}{\mu} & \dfrac{\bar{\omega}^2}{U_{m,nd}^2} & \dfrac{0.01365(1+\bar{u})}{\mu} & \dfrac{0.5020372}{\mu}\\
-(1+\bar{u}) & 0 & 0.01365 & 0\\
0 & 0 & 0 & 0.2510186
\end{bmatrix}
\begin{Bmatrix} \theta \\ \xi \\ z_1 \\ z_2 \end{Bmatrix}
=\begin{Bmatrix} 0 \\ 0 \\ 0 \\ \bar{w} \end{Bmatrix},
\tag{15}
$$

where $\bar{u}=u_T/U_m=u_{T,nd}/U_{m,nd}$ and $\bar{w}=w_T/U_m=w_{T,nd}/U_{m,nd}$.

Note that both the damping and stiffness matrices are time-varying or parametrically excited. This is due to the longitudinal turbulence excitation, which enters the problem by means of the aerodynamic loads. Longitudinal turbulence acts as a linear coloured random excitation on the damping terms via the normalized turbulent velocity $\bar{u}$. The excitation on the stiffness terms is both linear and quadratic, via $\bar{u}$ and $\bar{u}^2$, respectively. On the other hand, the mass matrix is time-invariant. The vertical component of turbulence acts as an external forcing function.

Solution of Eq. (15) is achieved by expressing it in state space form and solving it in the time domain using a standard fourth-order Runge-Kutta numerical integration scheme. Simultaneously, the turbulent velocity equations of motion, Eq. (8), which act as input to the aeroelastic equations, are also solved. In turn, the input to the turbulent velocity equations is a set of random numbers which are generated at each time step of the simulation. Accordingly, four statistically independent uniform deviates are produced using the routine RAN1 found in Press et al. (1996). The four uniform deviates are then transformed into two Gaussian distributed numbers using the Box-Muller algorithm (Knuth, 1998). This algorithm is the heart of a number of Monte Carlo simulations in the physics literature (Sancho et al., 1982; Fox et al., 1988; Fox, 1989). The simulation is run until steady state, in the statistical sense, is reached. The process is assumed to be ergodic, thus, providing an equivalency between ensemble and time averages. In this regard, all the dynamic information is contained in one sample response.

Because the Runge-Kutta method is an explicit integration scheme, the main requirement governing the time step is numerical stability. The time step of the integration is thus chosen as the minimum of either 1/50th of the nondimensional scale of turbulence, or noise correlation time, or 1/128th of the two uncoupled natural periods of the system.

The solution of the simulation is validated via a number of different criteria. First, it is confirmed that the solution is independent of the sample sequence of uniform random numbers. This is done by changing both the seed and the random number generator algorithm. Second, the variance, Gaussian distribution and PSD of the numerical solution of the turbulent velocities are checked against their pre-defined values. Third, the numerical solution of the aeroelastic system excited with pure vertical turbulence is compared with a closed-form frequency domain solution. Fourth, we check the convergence of the solution in terms of the time step. Numerical stability and accuracy of the response are verified. Finally, the Runge-Kutta solution of the aeroelastic system excited with both turbulent excitations, and then with pure longitudinal turbulence, is compared with Houbolt's method which is an implicit scheme. Except for the short transient phase, the two methods give indistinguishable results.

With regard to the numerical calculation of the largest Lyapunov exponent, we have tested its invariance with respect to initial conditions and sample noise realisations. All test runs resulted in the same (nonrandom) value, as expected from its theoretical foundations.

5. Results and discussion

As introduced earlier, the stability of the linear airfoil, strictly speaking the fixed point, is only affected by the longitudinal component of the turbulent excitation. The vertical component, which acts as an external forcing function, does not contribute to the loss of stability, but instead it affects the response level of the airfoil. This is a general property of linear dynamical systems and can be deduced from the definition of the Lyapunov exponent. Accordingly, unless otherwise specified, all results discussed in this paper have been obtained with pure longitudinal turbulent excitation.

5.1. Deterministic baseline

Throughout this paper, unless otherwise stated, results are given for the following set of nondimensional airfoil parameters: $\bar{\omega} = 0.6325$, $x_\theta = 0.25$, $r_\theta = 0.5$, $\mu = 100.0$, $a_h = -0.5$. Under these conditions (deterministic) flutter occurs at $U_{f,nd} = 4.31$ via mode 1. Mode 1 is defined as the mode with the lowest frequency, while mode 2 has the higher frequency. The loss of stability is exemplified in Fig. 3, which presents the behaviour of the two complex conjugate pairs of eigenvalues as a function of airspeed. The eigenvalues have been calculated using a standard eigenvalue analysis package. The flutter speed is given precisely at the airspeed where the real part of one of the eigenvalues changes sign, as shown in Fig. 3(a) by mode 1. Fig. 3(b) illustrates the coalescence of the two eigenfrequencies, whose values are given by the imaginary part of the eigenvalues. The flutter frequency is $k_f = 0.182$.

5.2. Influence of airfoil and Dryden turbulence parameters

As stated earlier, the random flutter point is determined according to a change in sign of the largest Lyapunov exponent. More precisely, $\lambda_{\max}$ is calculated numerically at different mean airspeeds until it changes from being negative (stable) to positive (unstable). For these calculations, the mean airspeed, $U_{m,nd}$, is swept with increments of 0.05. The random flutter speed, i.e. the mean airspeed at which $\lambda_{\max}$ is zero, is then interpolated between the pre- and post-flutter mean airspeeds (this is exemplified in Fig. 13).

According to this methodology, the accuracy of the flutter speed is determined by two factors: the error in the calculated largest Lyapunov exponent, and the subsequent interpolation. The error on $\lambda_{\max}$ is minimized by running the simulation until convergence is obtained within a tolerance of ± 0.00005, or $\pm 1\%$ to 10% of typical values of $\lambda_{\max}$ considered. When this error is combined with the interpolation process, the accuracy of the random flutter speed is estimated to be within ± 0.005, or $\pm 0.1\%$ of a typical flutter speed, for example $U_{m,nd} = 5.0 \pm 0.005$.

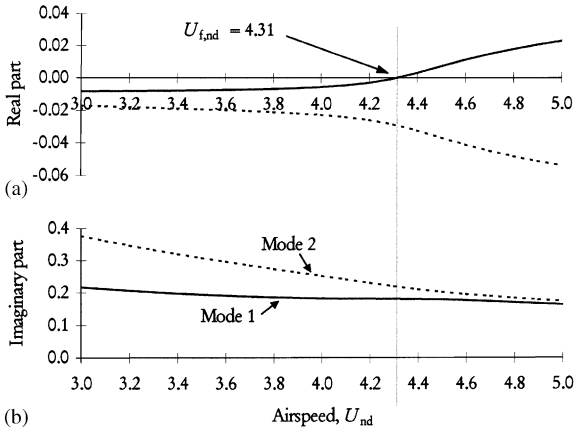

Fig. 3. Behaviour of the nonexcited (deterministic) airfoil eigenvalues as a function of airspeed; (a) real part (damping); (b) imaginary part (frequency).

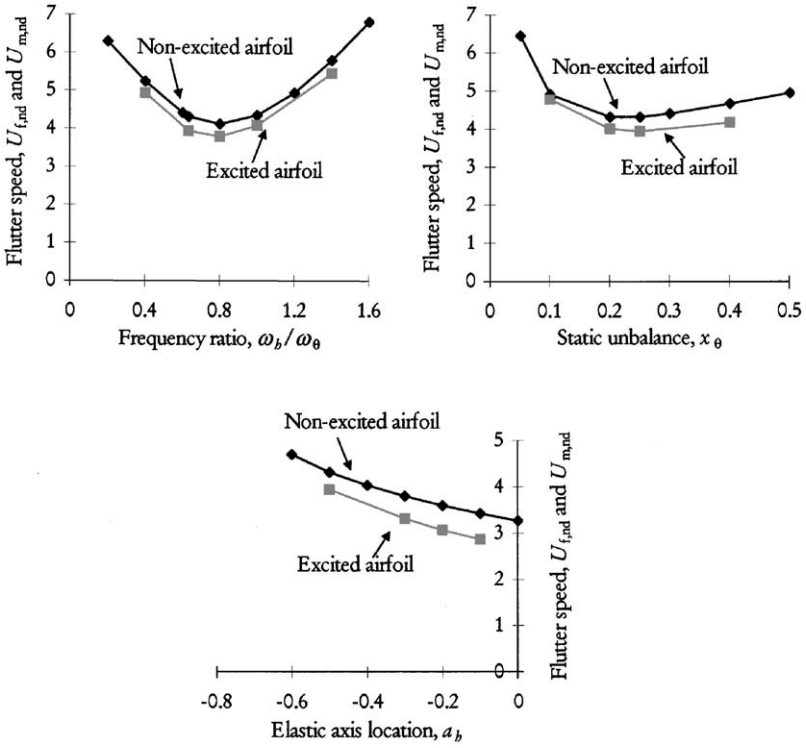

Fig. 4. Comparison of deterministic and random flutter boundaries for different combinations of airfoil parameters; $L_{nd} = 50.0$, $\sigma^2_{T,nd} = 0.5$; (a) $x_\theta = 0.25$, $a_h = -0.5$; (b) $\bar{\omega} = 0.6325$, $a_h = -0.5$; (c) $x_\theta = 0.25$, $\bar{\omega} = 0.6325$.

We have found that the flutter speed is systematically lowered by random turbulence, specifically its longitudinal component, for all airfoil and Dryden model parameters tested. The influence of the airfoil parameters is reported first. This is followed by a discussion of the effects of the turbulence parameters, namely variance and scale.

5.2.1. Sensitivity to frequency ratio, $\bar{\omega}$, static unbalance, x_θ, and elastic axis location, a_h

Fig. 4 shows the flutter speed as a function of either the frequency ratio, static unbalance or location of the elastic axis. It is observed that the flutter speed is systematically decreased by the presence of turbulence. Also of particular interest is that this reduction of the flutter speed occurs regardless of whether the heave or pitch DOF is stiffer; this is illustrated by the frequency ratio which is varied from smaller to larger than one. In turn this ratio, has an effect on which mode becomes unstable. For the baseline airfoil ($\bar{\omega} = 0.6325$) mode 1 is the unstable mode, whereas at $\bar{\omega} = 1.4$, for example, the airfoil loses stability via mode 2, which has the higher frequency.

5.2.2. Sensitivity to turbulence variance, $\sigma^2_{T,nd}$

The effect of turbulence level is demonstrated in Fig. 5, where the random flutter speed is plotted as a function of turbulence variance for four different scales of turbulence. The scale of turbulence ranges from a small scale at $L_{nd} = 0.5$, which effectively models white noise,[1] to a large scale at $L_{nd} = 50.0$. For all scales, the relationship between random flutter speed and turbulence variance is nearly linear. Note, as well, that the flutter speed decreases as the turbulence variance is increased.

Investigating the flutter airspeed–turbulence variance relationship further, we have found that for coloured noise the reduction in flutter speed is generally proportional to the area under the turbulence power spectral density, $\varphi_{LT,nd}(k)$, up to the deterministic (nonexcited) flutter frequency. This is illustrated in the following. Given that the turbulence

[1] It can be shown that the noise correlation time of the excitation, in nondimensional form, is equal to the scale of turbulence. Assuming that the flutter frequency, more precisely its inverse, is a representative time scale of the aeroelastic system, it is seen that $1/k_f \gg \tau_{cor}$ for $L_{nd} = 0.5$ (i.e. $1/0.182 = 5.5 \gg 0.5$). In other words, at this small value of scale of turbulence, the excitation spectrum is nearly flat for the range of frequencies to which the system potentially responds.

variance, $\sigma^2_{T,nd}$, is equal to the total area under the turbulence PSD, we define an effective variance, which in our case represents, loosely speaking, how much of the turbulence excitation participates in the reduction of the flutter speed. This is given by

$$\sigma^2_{\mathrm{eff},nd}(k) = \int_0^k \phi_{T,nd}(\kappa)\,\mathrm{d}\kappa. \tag{16}$$

For example, take a random flutter speed, $U_{m,nd} = 3.85$. From Fig. 5 it is deduced that the three sets of coloured turbulence parameters which correspond to that flutter speed are:

$\sigma^2_{T,nd} = 0.67, \quad L_{nd} = 50.0,$

$\sigma^2_{T,nd} = 1.0, \quad L_{nd} = 10.0,$

$\sigma^2_{Tnd} = 1.43, \quad L_{nd} = 5.0.$

The corresponding PSDs are plotted in Fig. 6, and the areas under each curve up to $k_f = 0.18$ are approximately the same and equal to $\sigma^2_{\mathrm{eff},nd} = 0.65$.

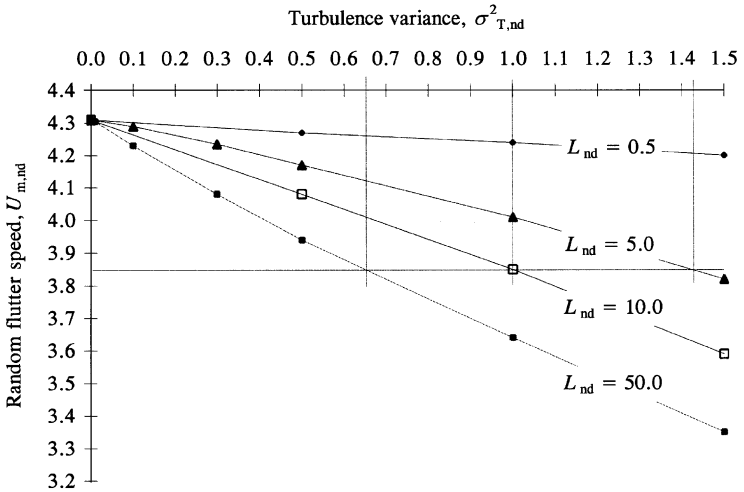

Fig. 5. Random flutter airspeed as a function of turbulence variance and for four scales of turbulence.

One immediate conclusion from this analysis is that the random flutter speed is essentially determined by the low frequency content of the excitation. This is generally the case for coloured excitation. However, for the smaller scale of turbulence, $L_{nd} = 0.5$, which acts effectively as "physical" white noise excitation, the same effective variance as for the larger scales is reached at a much higher frequency; thus, hinting to a sensitivity of the airfoil to a broader range of frequencies past the flutter frequency. A more detailed analysis of the effect of specific excitation frequencies is provided in Section 5.3.

5.2.3. *Sensitivity to scale of turbulence, L_{nd}*

Fig. 5 can be transformed to show more clearly the effect of scale of turbulence. In this regard, Fig. 7 indicates an asymptotic behaviour of the decrease in flutter speed as the scale of turbulence is increased past $L_{nd} = 50.0$. At this value of scale of turbulence, 95% of the turbulence power is located at frequencies lower than $k = 0.18$. Again, the deterministic flutter frequency appears to act as a useful reference frequency in terms of defining the region for low and very low frequencies that affect the stability.

A possible physical explanation of the enhanced sensitivity of the airfoil to low frequency parametric excitation is as follows. For large values of scale of turbulence, for which most of the excitation power is located in the low frequency range, and which are equivalent to large noise correlation times in comparison with the system time scales, the system has sufficient time to react and respond to the excitation. In other words, the excitation is temporarily frozen in time for the airfoil. Conversely, for small values of scale of turbulence the white noise idealization is approached. In this case, the noise varies so quickly that the system has no time to adjust, hence the airfoil is less affected by the turbulence.

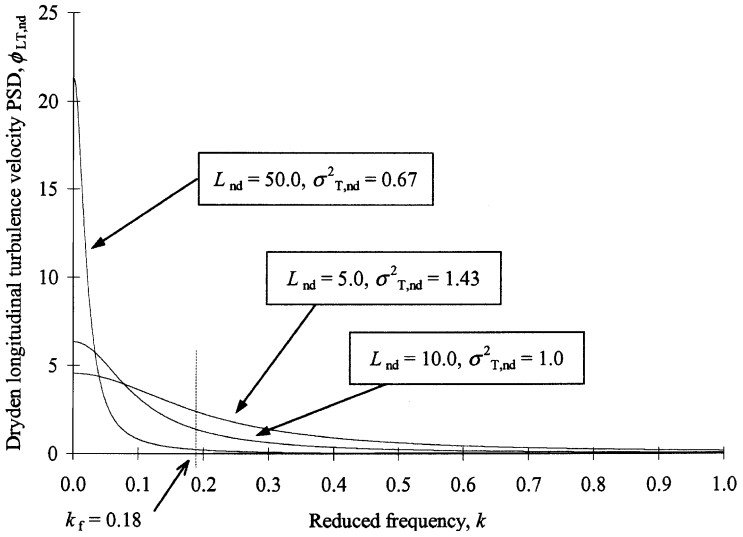

Fig. 6. Closed-form solutions of the nondimensional Dryden longitudinal turbulence velocity PSDs for different scales and variances, corresponding to the same random flutter speed, $U_{m,nd} = 3.85$.

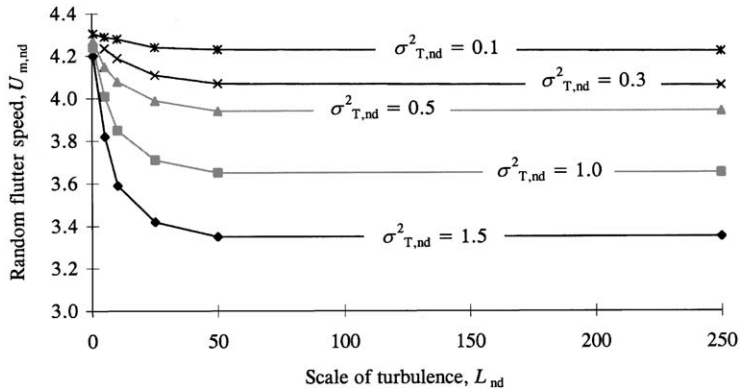

Fig. 7. Random flutter airspeeds as a function of scale of turbulence and for five values of turbulence variance.

5.3. Parametric resonance study

In the analysis of the previous section, the influence of the turbulent excitation was interpreted and described via an effective variance. This approach does not consider per se the excitation spectral density at specific critical frequencies; instead the excitation is viewed as a continuous low frequency band turbulence. Thus, this approach does not allow for a targeted analysis of the system sensitivity to a particular frequency band. A more profound understanding can be obtained by investigating the sensitivity of the stability to a narrow band parametric excitation. This is the subject of this section. In order to excite specific frequencies we have replaced the Dryden turbulence spectrum with the following narrow band model for the longitudinal excitation. The analytical expression for its PSD is given by the following equation: D controls the intensity (for a given ζ and r), ζ defines the width of the excitation band (for a given r), and the peak frequency is denoted by r.

$$\phi_{LT,nd}(k) = \frac{D}{(r^2 - k^2)^2 + (2\zeta r k)^2}, \tag{17}$$

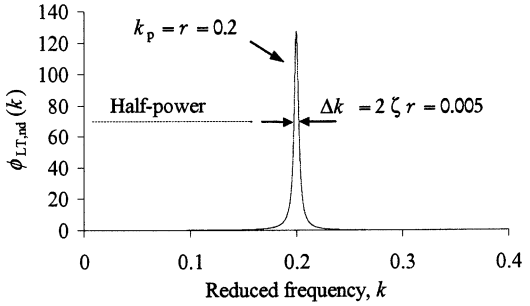

Fig. 8. Closed-form solution of the narrow band excitation PSD; $\zeta = 0.0125$, $r = 0.2$, $\sigma^2_{T,nd} = 1.0$.

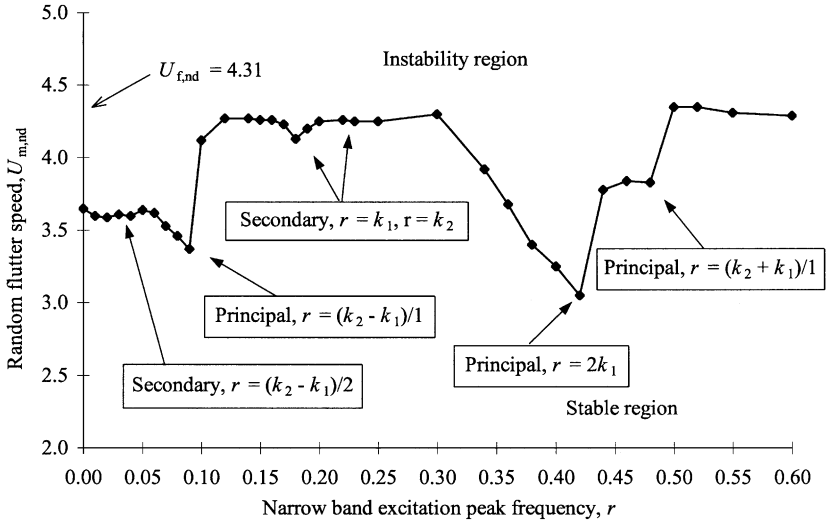

Fig. 9. Flutter boundary of the parametrically excited airfoil as a function of narrow band excitation peak frequency; $\sigma^2_{T,nd} = 1.0$, $\Delta k = 2\zeta r = 0.005$.

where (Newland, 1975):

$$D = \frac{2\zeta r^3}{\pi}\sigma^2_{T,nd} \tag{18}$$

Eq. (17) is represented graphically in Fig. 8. The time domain representation is given by

$$\mathrm{d}u'_{T,nd} + 2\zeta r u'_{T,nd}\,\mathrm{d}\tau + r^2 u_{T,nd}\,\mathrm{d}\tau = \sigma_{T,nd}\left(\frac{2\zeta r^3}{\pi}\right)^{1/2}\mathrm{d}W. \tag{19}$$

The stability of the airfoil as a function of this narrow band excitation is examined by sweeping the excitation peak frequency, r, from 0.01 to 0.60. The results are shown in Fig. 9 in the form of a stability boundary plot. In this process, the peak frequency is incremented nonuniformly; the increment, Δr, depends on the degree of resolution required for the stability boundary. Both the variance and bandwidth of the excitation are fixed for all peak frequencies. The variance is set at $\sigma^2_{T,nd} = 1.0$, and the bandwidth, defined at the half-power point as $\Delta k = 2\zeta r$, is kept constant at $\Delta k = 0.005$ by adjusting the value of the parameter ζ accordingly.

Before discussing the results shown in Fig. 9 it is relevant to point out that we are looking for parametric resonances. These resonances should appear as a dip in the stability boundary indicating a decrease of the flutter speed. Based on the deterministic flutter frequencies ($k_f \equiv k_1 \equiv 0.182$, $k_2 = 0.221$), we are therefore searching primarily for the following potential principal and secondary resonances. Note, a general observation is that principal resonances are more likely to occur than secondary resonances, and so on (Ibrahim, 1985; Cartmell, 1990; Lin, 1996).

Principal parametric resonances, $(k_i \pm k_j)/m$ where $i, j = 1, 2$ and $m = 1$:

$r = 2k_1 \rightarrow 0.36$

$r = 2k_2 \rightarrow 0.44$,

$r = k_2 + k_1 0.40$ (combination addition type),

$r = k_2 - k_1 \rightarrow 0.04$ (combination difference type).

Secondary parametric resonances, $(k_i \pm k_j)/m$ where $i, j = 1, 2$ and $m = 2$:

$r = k_1 \rightarrow 0.18$,

$r = k_2 \rightarrow 0.22$,

$r = (k_2 + k_1)/2 \rightarrow 0.20$ (combination addition type),

$r = (k_2 - k_1)/2 \rightarrow 0.02$ (combination difference type).

In light of these potential resonance conditions we now examine Fig. 9. Note that the solid line separates the stable region (below the curve) from the unstable airspeeds above it. In reference to the deterministic flutter speed, $U_{f,nd} = 4.31$, we denote six resonances. They are discussed as follows.

5.3.1. Principal parametric resonance, $2k_1$

The largest reduction in flutter speed occurs at $r \approx 0.42$. This excitation frequency appears to correspond to approximately twice the frequency of the second mode, $2k_2 \approx 0.44$. However, this value of k_2 is taken at the deterministic flutter speed, $U_{f,nd} = 4.31$. At the random flutter speed, $U_{m,nd} = 3.1$, its value has changed to $k_2 \approx 0.36$, while $k_1 \approx 0.21$. Accordingly, this resonance is more likely due to twice the frequency of the first mode, $2k_1 \approx 0.42$.

This excitation at $2k_1$ meets the condition of principal parametric resonance with the natural frequency of the flutter mode. In this light, we conclude that this resonance is the main cause of the sensitivity of the system to high excitation frequencies as observed with the Dryden model. It explains why the system is effectively excited by "physical" white noise, $L_{nd} = 0.5$, as discussed earlier. For larger values of scale of turbulence, this condition of principal parametric resonance still exists, but is much less dominant since the PSD of the Dryden model excitation at this frequency ($k \approx 0.42$) is relatively small compared with the low frequency excitation spectral density.

5.3.2. Principal parametric resonance, combination addition type, $(k_1+k_2)/1$

For frequencies slightly greater than $r = 0.42$ another resonance appears to be centred around $r \approx 0.47$. At this particular flutter speed ($U_{m,nd} = 3.8$), the possible principal resonances are: $r = 2k_2 = 2 \approx 0.275 = 0.55$ and $r = k_2 + k_1 = 0.275 + 0.187 = 0.462$. Consequently, the loss of stability in this region is more likely due to the principal parametric combination (addition type) resonance.

It is possible that the other principal resonance condition at $2k_2$ also affects the stability, but we believe its effect is so small compared to the other principal resonances at $2k_1$ and $k_2 + k_1$ that it is hidden within that large instability region centred around $r \approx 0.42$.

5.3.3. Principal parametric resonance, combination difference type, $(k_2-k_1)/1$

At $r = 0.09$ another strong resonance occurs. This is also a condition of principal parametric excitation, but since it is close to the condition $(k_2 - k_1)/1$ it corresponds to a combination difference type. As for the resonance at $r = 0.42$, when interpreting this result as being related to the difference of the two eigenfrequencies it should be realized that their values are more likely to be determined by the random flutter speed than the deterministic one. At $U_{m,nd} = 3.35$, the difference between the deterministic eigenfrequencies is: $k_2 - k_1 = 0.325 - 0.20 = 0.125$ compared with 0.04 at $U_{f,nd} = 4.31$.

5.3.4. Secondary parametric resonances, $2k_1/2$ and $2k_2/2$

Turning our attention to the secondary parametric excitation frequencies, we note a small region of destabilization centred at $r = 0.18$, and to its right a hint of resonance at $r = 0.22$. These conditions correspond to two secondary (noncombination) parametric resonances. It is not surprising that their strengths are smaller than the principal parametric resonance discussed earlier. Support for this hypothesis comes from Ibrahim (1985) who discusses the problem of a single-degree-of-freedom system in conditions of random parametric excitation, where the loss of stability

for the principal parametric resonance (excitation frequency is twice the system natural frequency) is much more important than for the secondary parametric condition. In our case, and comparing these two secondary resonances, we also point out that the strongest of the two appears at k_1, which is the flutter frequency.

5.3.5. Secondary parametric resonance, combination difference type, $(k_2-k_1)/2$

The last region where a decrease in stability is observed is relatively broad and covers the range of very small frequencies. Its existence can be explained by two mechanisms. First, there exists a condition of secondary combination difference resonance, which based on the random flutter speed, $U_{m,nd} = 3.6$, gives $(k_2 - k_1)/2(0.29-0.19)/2 = 0.05$. The second mechanism is related to the value of the PSD at zero frequency. It has been shown analytically that this condition is a determinant in the stability of a single-degree-of-freedom system (Lin, 1996; Ariaratnam and Tam, 1979). However, it was also shown that the loss of stability at this condition originated from the random damping term, i.e. when the random excitation acts on the damping. In our case, however, we will argue in Section 5.4 that the damping terms have a secondary effect on the random flutter mechanism. Consequently, the first cause is probably the most important.

In summary, we have observed two broad regions of particular sensitivity, or strong resonances, to narrow band excitation. One, located in either the very low or low frequency range, is determined by the secondary and principal combination, difference type, parametric resonances, $(k_2 - k_1)/2$ and $(k_2 - k_1)/1$, respectively. The other region is centred around the principal parametric resonance, $2k_1$, with contributions from the principal combination, addition type, parametric resonance $(k_2 + k_1)/1$, and the other principal parametric resonance at $2k_2$.

These resonances have a particular significance for coalescence flutter. The inherent nature of coalescence flutter is to have two closely spaced frequencies, i.e. $k_2 \approx k_1$ (where $k_1 \equiv k_f$). One important consequence of the coalescence is that the two combination, difference type, parametric resonances, $(k_2 - k_1)/2$ and $(k_2 - k_1)/1$, are located close to each other, and also close to zero. This explains the significant decrease in flutter speed when the airfoil is parametrically excited with the low band Dryden turbulence, since most of the excitation power is located in the very low frequencies.

Another consequence of having two closely spaced frequencies is that the principal parametric resonances at $2k_1$, $2k_2$, and $k_2 + k_1$, are also in close proximity to each other. These conditions combine to form a large region of destabilization for "physical" white noise excitation, i.e. for small values of scale of turbulence.

In contrast, for the case of single-degree-of-freedom flutter reported by Lin and Li (1993); Li and Lin (1995); Lin (1996), and discussed in Section 2 of this paper, there is no frequency coalescence. For this single-degree-of-freedom instability there is one main condition of principal parametric resonance at $2k_f$, and possibly at $2k_2$ and combination resonances if coupling is introduced with another degree-of-freedom. However, since there is no coalescence, the aeroelastic frequencies are, in general, well separated and the region(s) of parametric resonance is(are) therefore narrow and not necessarily close to the zero frequency axis. In comparison with the problem investigated in this paper, results from Lin and Li for a two-degree-of-freedom analysis of single-degree-of-freedom, negative-damping, flutter indicate a narrow unstable region centred at $2k_1$, none at $2k_2$, and a relatively smaller unstable region at $k_1 - k_2$. Their results also suggest a light sensitivity of the system to principal parametric combination (addition type) resonance, $k_2 + k_1$.

5.4. Aspects of frequency coalescence

5.4.1. General considerations

The findings reported in this section build on, and clarify, some of the results communicated in a previous paper (Poirel and Price, 2001), where for airspeeds approaching the flutter condition we discussed difficulties in interpreting the frequency content of the linear airfoil response to combined turbulence. These difficulties were attributed to the very low damping of the slow mode, and, hence, extreme sensitivity to perturbations. In this paper, we have refined our analysis, and show that the phenomenon of frequency coalescence, a fundamental element of the deterministic flutter instability, plays a role in the decrease of the random flutter speed. More particularly it is observed that longitudinal excitation modifies the system modal characteristics, and, in turn, the frequency coalescence.

In order to study the influence of the longitudinal turbulent excitation on the frequency coalescence, the simulation is run at pre-flutter airspeeds, and the (stationary) spectral response of the airfoil to vertical turbulence is examined. A visual interpretation of the two aeroelastic modal frequencies can then be obtained relatively easily. For this analysis the use of the vertical turbulent excitation is required not to investigate its effect on the airfoil response, but as a means of exciting the system and probing its dynamics. In this respect it should be remembered that the (stable) linear airfoil cannot have sustained behaviour unless it is excited by an external forcing.

Fig. 10 shows a comparison of the closed-form solution obtained directly in the frequency domain with the spectral representation of the numerical time domain solution for the airfoil excited by pure vertical turbulence. The scale of turbulence is $L_{nd} = 0.5$, which effectively models "physical" white noise. The closed-form and numerical solution PSDs

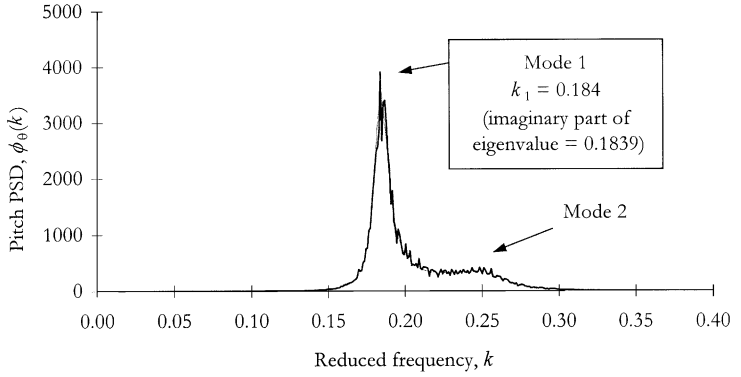

Fig. 10. Comparison of numerical (▬) and closed-form (—) solution PSDs of the pitch response to pure vertical turbulence; $\sigma^2_{T,nd} = 1.0$, $L_{nd} = 0.5$, $U_{nd} = 4.0$.

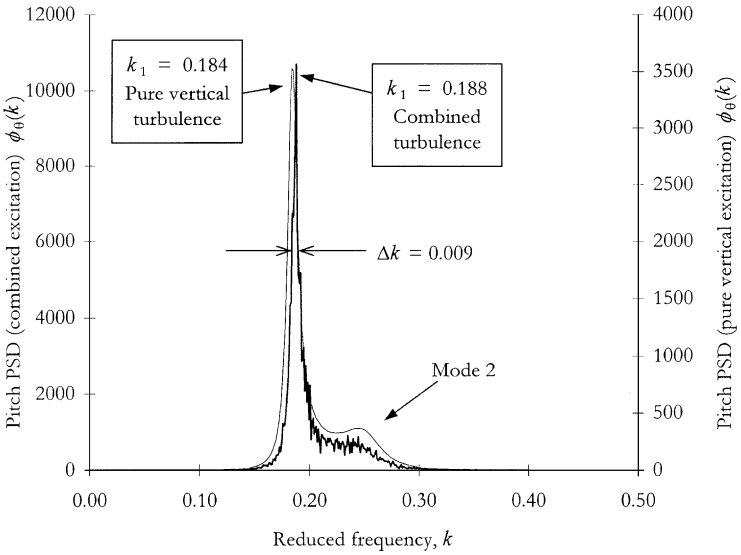

Fig. 11. PSD plot of the airfoil pitch response to combined excitation turbulence (numerical solution, ▬) and pure vertical turbulence (closed-form solution, —) at $U_{m,nd} = 4.0$; $\sigma^2_{T,nd} = 1.0$, $L_{nd} = 0.5$.

are nearly indistinguishable, except for local variations in the numerical based spectrum; the minor differences are attributed to the discretization process of the Fourier transform and can be diminished by taking more averages. Note that the PSD shown for the numerical solution represents an average of 59 fast Fourier transforms (FFT) for sequential time samples, each composed of 65,536 (i.e. $N_{\mathrm{FFT}} = 2^{16}$) data points; this represents approximately 4 million data points used to estimate the spectral response. The almost perfect match between the overall contour of the numerical based PSD and the closed-form solution validates the numerical solution from the points of view of both the numerical integration and the calculation of the FFT. Furthermore, the peak in the numerical based spectrum is located at $k = 0.184$; the frequency resolution is $\Delta k = 0.00096$ (i.e.$\Delta k = 2\pi/(N_{\mathrm{FFT}}\Delta T)$ where $N_{\mathrm{FFT}} = 2^{16}$ and the integration time step $\Delta T = 0.1$). In comparison, the eigenfrequency obtained with a standard eigenvalue analysis is $k = 0.1839$; see Fig. 3(b) for mode 1. These are essentially identical.

In Fig. 11, the same closed-form solution is compared with the numerical based PSD for the airfoil excited with both vertical *and* longitudinal turbulence. In comparison with the case for pure vertical excitation, we observe a clear narrowing of the dominant mode accompanied by an increase in frequency at which the maximum response occurs. This dominant mode represents the slow linear mode (mode 1).

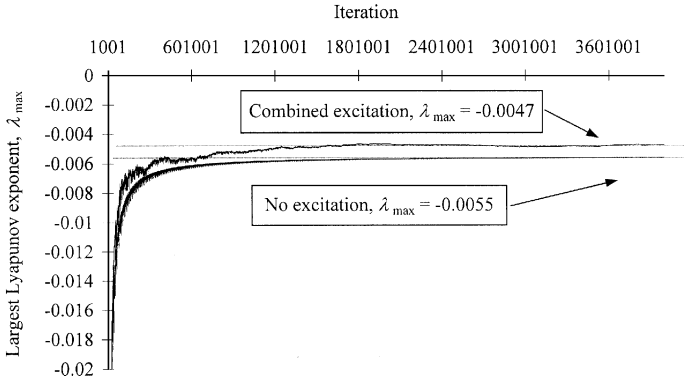

Fig. 12. Time (iteration) evolution of the largest Lyapunov exponent of the nonexcited airfoil and in combined excitation turbulence at $U_{m,nd} = 4.0$; $\sigma^2_{T,nd} = 1.0$, $L_{nd} = 0.5$.

Due to the longitudinal turbulence, mode 1 is shifted from $k_1 = 0.184$ to $k_1 = 0.188$, hence towards the second mode. Although not evident from Fig. 11, since at this airspeed the PSD is dominated by the mode losing stability (mode 1), mode 2 is also shifted by the longitudinal turbulence but in this case to a lower frequency. At lower airspeeds, where mode 2 is more clearly defined, the shift is more easily seen. For example, at $U_{m,nd} = 3.5$ mode 2 is shifted from $k_2 = 0.308$ to $k_2 = 0.299$ by the longitudinal turbulence. Furthermore, changing the frequency ratio such that heave is stiffer than pitch does not change this behaviour. For example, as opposed to the baseline airfoil ($\bar{\omega} = 0.6325$) which loses stability via mode 1, the mode losing stability for the airfoil with $\bar{\omega} = 1.4$ is the second mode. In this case mode 2 is also shifted toward smaller frequencies, hence toward coalescence.

As noted above, we have observed that longitudinal turbulence causes a systematic shift of both modes towards each other. We conclude by arguing that the observed increase of the first modal frequency combined with a decrease of the second modal frequency is an indication that longitudinal turbulence advances the frequency coalescence. We can also interpret this observation in the sense that longitudinal turbulence increases the coupling between the pitch and heave motion.

The PSD of the linear response to combined turbulence excitation contains not only information on the system natural frequencies, but also on its modal damping. Hence, from the narrowing of the peak, it is concluded that the modal damping for mode 1 is decreased by the presence of longitudinal turbulence. This is coherent with the observation that the flutter speed is lowered, since a reduction in damping is characteristic of approaching the instability point. Also shown is the width of the dominant mode at the half-power point, $\Delta k_{1/2\mathrm{PSD}}$; taking half of this parameter (i.e. $\Delta k_{1/2\mathrm{PSD}}/2$) and interpreting it as the real part of the eigenvalue for mode 1 (with longitudinal excitation), we have:

$$-\zeta_1 k_1 = -\Delta k_{1/2\mathrm{PSD}}/2 = -0.009/2 = -0.0045.$$

This value is compared with the largest Lyapunov exponent at the same speed, $\lambda_{\max}$ ($U_{m,nd} = 4.0$) $= -0.0047$; see Fig. 12. This comparison provides a physical understanding of the concept of the largest Lyapunov exponent in the context of longitudinal excitation. Note that both a standard eigenvalue analysis, see Fig. 3(a), and the numerically calculated largest Lyapunov exponent, as shown in Fig. 12, indicate that the real part of the equivalent deterministic eigenvalue is $\lambda_1 = -0.0055$, thus indicating more damping for the nonexcited airfoil.

5.4.2. *Sensitivity to random stiffness and damping terms*

The frequency coalescence question can also be elucidated by examining the sensitivity of the decrease of the flutter speed to the random stiffness terms, and in corollary to the random damping terms. Due to the inherent stiffness-controlled nature of the frequency coalescence phenomenon associated with classical binary flutter, it is shown that the random stiffness terms are essential contributing factors, whereas the random terms in the damping matrix do not significantly influence the flutter point.

Fig. 13 illustrates the relative importance of random stiffness and random damping terms via the behaviour of the largest Lyapunov exponent. Four cases are shown based on the following airfoil parameters $\bar{\omega} = 0.6325$, $x_\theta = 0.25$, $r_\theta = 0.5$, $\mu = 100.0$, $a_h = -0.2$. The deterministic, nonexcited, airfoil has a flutter speed of $U_{f,nd} = 3.59$. The excited airfoil, with turbulence variance $\sigma^2_{T,nd} = 0.5$ and scale $L_{nd} = 50.0$, flutters at $U_{m,nd} = 3.07$. In between these two extremes are two situations, in one case the random terms in the damping matrix of Eq. (15) are artificially neutralized, and in the

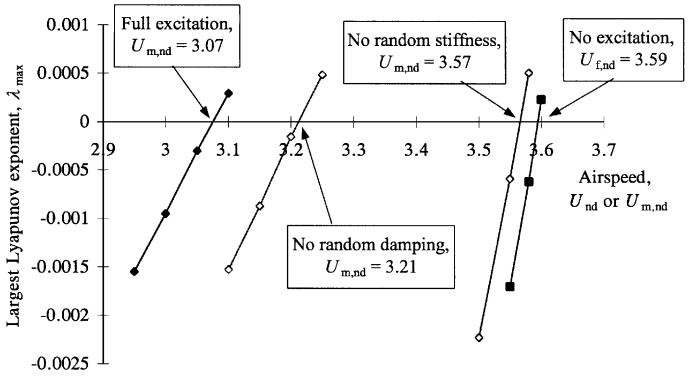

Fig. 13. Largest Lyapunov exponent as a function of mean airspeed in longitudinal turbulence with random damping and stiffness terms switched on and off, and nonexcited; $\sigma^2_{T,nd} = 0.5$, $L_{nd} = 50.0$ and $\bar{\omega} = 0.6325$, $x_\theta = 0.25$, $r_\theta = 0.5$, $\mu = 100.0$, $a_h = -0.2$.

other case the random terms in the stiffness matrix are set to zero. It is clear that the random terms in the aeroelastic system stiffness matrix have much more impact on the decrease of stability, and associated lowering of the flutter speed, than the random damping terms. We conclude by arguing that this observation confirms the nature of the shift in flutter speed to be stiffness controlled, as is the case for the deterministic part. It is also an indirect indication that the coalescence of the two frequencies involved in flutter is modified by longitudinal turbulence.

6. Conclusion

We have found that the flutter speed of a two-degree-of-freedom airfoil is systematically decreased by random turbulence, specifically its longitudinal component, for all airfoil and Dryden turbulence model parameters tested. This has been shown to be the case for different combinations of frequency ratio, static unbalance or location of the elastic axis, as well as for a large range of variance and scale of turbulence.

The relationship between random flutter speed and turbulence level (as defined by its variance) is nearly linear. Furthermore, for a realistic turbulence spectrum, i.e. away from the white noise idealization, the decrease in flutter speed is approximately proportional to the area under the longitudinal excitation PSD curve up to the flutter frequency.

It has been shown that the value of the parametric excitation PSD at frequencies corresponding to the principal, $k_2 - k_1$, and secondary, $(k_2 - k_1)/2$, combination difference type parametric resonances are critical factors for the decrease in stability. This has particular significance for the coalescence flutter mechanism where the excitation originates from turbulence, since these two specific elements (difference combination resonance of two close frequencies and large excitation for small frequencies) combine to essentially determine the magnitude of the decrease. For the "physical" white noise spectrum, the two parametric resonance conditions at $2k_1$ and $k_2 + k_1$ also become important.

The system modal characteristics (eigenvalues) are modified by longitudinal turbulence, which acts as a parametric excitation. In particular, we have observed a systematic shift of both eigenfrequencies towards each other, such that frequency coalescence occurs at a lower airspeed. Associated with a change in modal frequencies is a decrease in damping of the slow mode due to longitudinal turbulence, as indicated by both the largest Lyapunov exponent and the width of the dominant mode at the half-power point as obtained from the response PSD.

The degree of stability of the turbulent excited airfoil, as well as the random flutter speed itself, is dictated in a large part by the random stiffness terms, whereas the random damping terms have a secondary influence. The nature of the shift of the flutter point is, thus, essentially stiffness related. This is interpreted as another indication that the stiffness-controlled frequency coalescence is modified by longitudinal turbulence.

References

Ariaratnam, S.T., Tam, D.S.F., 1979. Random vibration and stability of a linear parametrically excited oscillator. ZAMM 59, 79–84.

Arnold, L., 1995. Random dynamical systems. In: Dynamical Systems (Lectures given at the 2nd session of the CIME). Verlag, Berlin, pp. 1–43.

Arnold, L., 1998. Random Dynamical Systems. Verlag, Berlin.

Arnold, L., Kliemann, W., Oeljeklaus, E., 1986. Lyapunov exponents of linear stochastic systems. In: Proceedings of a Workshop on Lyapunov Exponents (Lecture Notes in Mathematics) 1186. Verlag, Berlin, pp. 85–125.

Baxendale, P., 1991. Invariant measures for nonlinear stochastic differential equations. In: Proceedings of a Conference on Lyapunov Exponents (Lecture Notes in Mathematics) 1486. Verlag, Berlin, pp. 123–140.

Bucher, C.G., Lin, Y.K., 1988a. Effect of spanwise correlation of turbulence field on the motion stability of long-span bridges. Journal of Fluids and Structures 2, 437–451.

Bucher, C.G., Lin, Y.K., 1988b. Stochastic stability of bridges considering coupled modes. ASCE Journal of Engineering Mechanics 114, 2055–2071.

Bucher, C.G., Lin, Y.K., 1989. Stochastic stability of bridges considering coupled modes: II. ASCE Journal of Engineering Mechanics 115, 384–400.

Cartmell, M., 1990. Introduction to Linear, Parametric and Nonlinear Vibrations. Chapman and Hall, London.

Dinyavari, M.A.H., Friedmann, P.P., 1986. Application of time-domain unsteady aerodynamics to rotary-wing aeroelasticity. AIAA Journal 24, 1424–1432.

Done, G., 1996. Past and future progress in fixed and rotary wing aeroelasticity. Aeronautical Journal 100, 269–279.

Fox, R.F., 1989. Numerical simulations of stochastic differential equations. Journal of Statistical Physics 54, 1353–1366.

Fox, R.F., Gatland, I.R., Roy, R., Vemuri, G., 1988. Fast, accurate algorithm for numerical simulation of exponentially correlated colored noise. Physical Review A 38, 5938–5940.

Fujimori, Y., Lin, Y.K., Ariaratnam, S.T., 1979. Rotor blade stability in turbulent flows—part II. AIAA Journal 17, 673–678.

Fung, Y.C., 1955. An Introduction to the Theory of Aeroelasticity. Wiley, New York.

Hoblit, F., 1988. Gust Loads on Aircraft: Concepts and Applications. AIAA, Inc, Washington, DC.

Houbolt, J., Steiner, R., Pratt, K., 1964. Dynamic response of airplanes to atmospheric turbulence including flight data on input and response. NASA Tech. Rep. R-199.

Ibrahim, R.A., 1985. Parametric Random Vibration. Research Studies Press, Ltd, Letchworth.

Ibrahim, R.A., Orono, P.O., 1991. Stochastic non-linear flutter of a panel subjected to random in-plane forces. International Journal of Non-Linear Mechanics 26, 867–883.

Ibrahim, R.A., Orono, P.O., Madaboosi, S.R., 1990. Stochastic flutter of a panel subjected to random in-plane forces part I: two mode interaction. AIAA Journal 28, 694–702.

Knuth, D.E., 1998. The Art of Computer Programming, Vol. 2. Addison Wesley Longman, Inc., Reading, MA.

Li, Q.C., Lin, Y.K., 1995. New stochastic theory for bridge stability in turbulent flow II. ASCE Journal of Engineering Mechanics 121, 102–116.

Lin, Y.K., 1996. Stochastic stability of wind-excited long-span bridges. Probabilistic Engineering Mechanics 11, 257–261.

Lin, Y.K., Li, Q.C., 1993. New stochastic theory for bridge stability in turbulent flow. ASCE Journal of Engineering Mechanics 119, 113–127.

Lin, Y.K., Fujimori, Y., Ariaratnam, S.T., 1979. Rotor blade stability in turbulent flows—Part I. AIAA Journal 17, 545–552.

Newland, D.E., 1975. An Introduction to Random Vibrations and Spectral Analysis. Longman Group, Ltd, London.

Mitchell, R.R., Kozin, F., 1974. Sample stability of second order linear differential equations with wide band noise coefficients. SIAM Journal of Applied Mathematics 27, 571–605.

Poirel, D., 2001. Random dynamics of a structurally airfoil in turbulent flow. Ph.D. Dissertation, Department of Mechanical Engineering, McGill University, Montréal, Québec, Canada.

Poirel, D., Price, S.J., 1997. Post-instability behavior of a structurally nonlinear airfoil in longitudinal turbulence. Journal of Aircraft 34, 619–626.

Poirel, D., Price, S.J., 2001. Structurally nonlinear fluttering airfoil in turbulent flow. AIAA Journal 39, 1960–1968.

Press, W.H., Flannery, B.P., Teukolsky, S.A., Vetterling, W.T., 1996. Numerical Recipes in Fortran 77: The Art of Scientific Computing. Cambridge University Press, Cambridge.

Prussing, J.E., Lin, Y.K., 1982. Rotor blade flap-lag stability in turbulent flows. Journal of the American Helicopter Society 27, 51–57.

Prussing, J.E., Lin, Y.K., 1983. A closed-form analysis of rotor blade flap-lag stability in hover and low-speed flight in turbulent flow. Journal of the American Helicopter Society 28, 42–46.

Romberg, O., Popp, K., 1998. The influence of upstream turbulence on the stability boundaries of a flexible tube in a bundle. Journal of Fluids and Structures 12, 153–169.

Sancho, J.M., San Miguel, M., Katz, S.L., Gunton, J.D., 1982. Analytical and numerical studies of multiplicative noise. Physical Review A 26, 1589–1609.

van der Wall, B.G., Leishman, J.G., 1994. On the influence of time-varying flow velocity on unsteady aerodynamics. Journal of the American Helicopter Society 39, 25–36.